PHYSICAL REVIEW B VOLUME 27, NUMBER 6 15 MARCH 1983

Far-infrared absorption spectrum of excitons in [111]-stressed germanium: High-stress limit

D. Labrie and T. Timusk
Department of Physics, McMaster University, Hamilton, Ontario L8S 4M1, Canada
(Received 1 November 1982)

A series of experiments were performed to study the far-infrared absorption spectrum of excitons in stressed Ge with the stress axis along the [111] direction. The spectra were taken with stress ranging from 9 to 38 kg/mm^2 and with polarization of the far-infrared electric field parallel and perpendicular to the stress axis. The $1S$-$2P$ and $1S$-$3P$ transitions were observed. The line positions and the relative absorptions associated with the $1S$-$2P$ transitions are in good agreement with a simple theoretical model. The model only considers the lower conduction-band minima and the upper valence-band maxima at high stress in the formation of excitons. The binding energy of excitons at infinite stress is 2.70 ± 0.08 meV.

I. INTRODUCTION

The most fruitful information on the quantum structure of excitons in germanium was obtained by the far-infrared (FIR) absorption experiments.[1–7] In these experiments, the transitions from the $1S$ to $2P$ states were observed. Furthermore, the $1S$ state binding energies were measured by Sidorov and Pokrovskii[8] who examined the FIR exciton photoconductivity, and by Frova *et al.*[9] who looked at the derivative of the absorption edge. An energy spectrum of the low-lying levels was, therefore, constructed experimentally. A comprehensive theoretical treatment of the exciton energy spectrum was made by Lipari *et al.*[10–12] Despite the complicated band structure, good agreement between calculated and measured energy levels was obtained. Nevertheless, there are some transitions observed which are not predicted and some of the predicted transitions have not been observed.

Applications of a uniaxial stress along the [111] direction simplifies the band structure. At very large stresses, the excitons are formed from one conduction band and one valence band. Both bands are ellipsoids of revolution with their major axis along the [111] direction. The resulting energy spectrum of excitons is very simple. Muro *et al.*[13] and Yamanaka *et al.*[14] determined from their FIR magnetoabsorption of excitons at intermediate stresses a ground-state energy of ≈ 2.75 meV. Feldman *et al.*[15,16] measured from luminescence experiments at intermediate stresses a binding energy of 2.3 ± 0.4 and 2.6 ± 1.2 meV, respectively. These experiments were not able to establish the exciton spectrum at very large stresses.

In this paper, we examine the FIR absorption spectrum of excitons at very large stresses. A theoretical model is used to predict the energy levels and the relative absorption of transition lines. The method of calculation and the numerical results are given in the next section. The absorption spectra were measured as a function of stress from 9 to 38 kg/mm^2 and as a function of the direction of the FIR polarization with respect to the stress axis. At high stress, the exciton spectra are similar to the observed donor spectra. The results are presented with a comparison of the model in Sec. IV. Good agreement is observed between theory and experiment.

II. THEORY

In the absence of stress, excitons are formed from electrons of the first conduction-band minima and from holes of the valence-band edge. The conduction-band minima are located at the zone boundary of the first Brillouin zone along the $\langle 111 \rangle$ directions. The valence band is fourfold degenerate ($J=\frac{3}{2}$) at $\vec{k}=0$. At $\vec{k}$ different than zero, the band edge splits into a heavy-hole band $M_J=\pm\frac{1}{2}$ and a light-hole band $M_J=\pm\frac{3}{2}$.

Application of a uniaxial compressive stress S along the [111] direction reduces the cubic symmetry of the crystal and therefore removes some of the band degeneracies. The conduction-band ellipsoid whose major axis is along the [111] direction is lowered in energy with respect to the three others. The separation between the upper and lower valleys is $\Delta_e=1.03\,|S|$ meV/(kg/mm^2).[17] The valence band $J=\frac{3}{2}$ splits into two doubly degenerate states $M_J=\pm\frac{1}{2}$ and $M_J=\pm\frac{3}{2}$. As a function of stress the

heavy-hole band $M_J=\pm\frac{1}{2}$ goes up in energy relative to the light-hole band $M_J=\pm\frac{3}{2}$. The stress dependence of their separation is $\Delta_h=0.366|S|$ meV/(kg/mm^2).[18] Despite their splitting at $\vec{k}=0$ significant coupling between the bands remains until large stresses. In the limit of high stresses, the hole bands become ellipsoids of revolution with their major axis along the [111] direction. The effective masses of the valence bands were measured by Hensel *et al.*[18] They also observed the effective masses of the conduction band do not vary with stress. Hence, the effective masses of the conduction band measured by Levinger *et al.*[19] will be used in the following calculation.

In the effective-mass approximation the exciton Hamiltonian is

$$H_{\rm ex}=H_e(\vec{p}_e)+H_h(\vec{p}_h)-\frac{e^2}{\epsilon_0|\vec{r}_e-\vec{r}_h|}\ , \tag{1}$$

where the subscripts e and h, respectively, refer to the electron and hole, $\vec{p}$ is the momenta conjugate to $\vec{r}$, and ϵ_0 is the static dielectric constant. At very large stress $H(\vec{p})$ in the above equation takes the form

$$H(\vec{p})=\frac{1}{2m_t}(p_1^2+p_2^2)+\frac{1}{2m_l}p_3^2\ , \tag{2}$$

where m_l and m_t are the longitudinal and transverse masses, respectively, and p_3 is the momentum component along the [111] direction. To solve the Schrödinger equation associated with Hamiltonian (1), we make the following transformation of coordinates (Altarelli *et al.*[11]):

$$\begin{aligned}\vec{r}&=\vec{r}_e-\vec{r}_h\ ,\\ \vec{R}&=\alpha\vec{r}_e+\beta\vec{r}_h\ ,\end{aligned} \tag{3}$$

where α and β are 3×3 matrices and α and β satisfy $|\det(\alpha+\beta)|=1$. The conjugate momenta are given by

$$\begin{aligned}\vec{p}_e&=\alpha\vec{P}+\vec{p}\ ,\\ \vec{p}_h&=\beta\vec{P}-\vec{p}\ .\end{aligned} \tag{4}$$

By analogy to the hydrogen problem, we choose

$$\alpha=\begin{bmatrix} m_{et}/M_t & 0 & 0\\ 0 & m_{et}/M_t & 0\\ 0 & 0 & m_{el}/M_l\end{bmatrix},\qquad \beta=\begin{bmatrix} m_{ht}/M_t & 0 & 0\\ 0 & m_{ht}/M_t & 0\\ 0 & 0 & m_{hl}/M_{hl}\end{bmatrix}, \tag{5}$$

where $M_t=m_{et}+m_{ht}$, $M_l=m_{el}+m_{hl}$, and $|\det(\alpha+\beta)|=1$ is satisfied. The exciton Hamiltonian becomes

$$\begin{aligned}H_{\rm ex}&=\left[\frac{P_1^2+P_2^2}{2M_t}+\frac{P_3^2}{2M_l}\right]+\left[\frac{p_1^2+p_2^2}{2\mu_t}+\frac{p_3^2}{2\mu_l}-\frac{e^2}{\epsilon_0 r}\right]\\ &=H_{\rm c.m.}+H_r\ ,\end{aligned} \tag{6}$$

where

$$\mu_l^{-1}=m_{el}^{-1}+m_{hl}^{-1}$$

and

$$\mu_t^{-1}=m_{et}^{-1}+m_{ht}^{-1}\ .$$

We now introduce the effective Rydberg and the effective Bohr radius,

$$R_0=\frac{\mu_t e^4}{2\hbar^2\epsilon_0^2},\quad a_0=\frac{\hbar^2\epsilon_0}{\mu_t e^2}\ , \tag{7}$$

as units of energy and length, respectively. H_r expressed in reduced units becomes

$$H_r=-\left[\frac{\partial^2}{\partial x^2}+\frac{\partial^2}{\partial y^2}+\gamma\frac{\partial^2}{\partial z^2}\right]-\frac{2}{(x^2+y^2+z^2)^{1/2}}\ , \tag{8}$$

where $\gamma=\mu_t/\mu_l$. By using the electron and hole effective masses of Levinger *et al.*[19] and Hensel *et al.*,[18] respectively, and the static dielectric constant of Faulkner,[20]

$$\begin{aligned}\gamma&=1.275\ ,\\ R_0&=2.889\ ,\\ a_0&=162.2\end{aligned} \tag{9}$$

with R_0 in meV and a_0 in Å. The Hamiltonian H_r given in Eq. (8) for the relative motion of exciton in the high-stress limit is formally identical to the donor Hamiltonian. The donor problem was first analyzed by Kohn and Luttinger.[21] They observed that H_r is invariant under a rotation around the z axis and under inversion, hence, the z component of the angular momentum m and the parity P are conserved. However, all states with the same m and P are mixed. They calculated with a variational method the $1S$, $2P_0$, $2P_\pm$, $2S$, and $3P_0$ energy levels by using a single trial function for each eigenfunction. The subscripts 0 and $\pm$ stand for $m=0$ and $m=\pm1$. Faulkner[20] solved the problem by expanding each eigenfunction into a linear combination of trial functions. However, these authors treated the

problem for $\gamma \leq 1$ whereas for the exciton problem, $\gamma = 1.275$. Keyes[22] repeated the calculation of Kohn and Luttinger only for the $1S$ level with $\gamma \geq 1$ and with an anisotropic, static dielectric constant. We reproduced Kohn and Luttinger's variational calculation for the $1S$, $2P_0$, and $2P_\pm$ levels for $\gamma \geq 1$. These single variational wave functions represent very well these low-lying levels.[20] Nevertheless, this method yields only upper bounds of the energy levels.

The calculated $1S$, $2P_0$, and $2P_\pm$ energy levels as a function of γ are shown in Fig. 1. From Fig. 1, the $2P_0$ energy level lies higher in energy than the $2P_\pm$ level. Therefore, the line center of the $1S$-$2P_0$ transition ν_0 will be in the high-energy side of the line center of the $1S$-$2P_\pm$ transition $\nu_\pm$. The line positions are inverted with respect to the donor ones. This line inversion is easily understood since for $\gamma > 1$, $\mu_t > \mu_l$ hence, the transverse component of the kinetic energy is smaller than the longitudinal one. The resulting binding energy of the $2P_\pm$ state will be bigger than the $2P_0$ state.

To have an estimate of the strength of the $1S$-$2P$ transitions, one can evaluate the relative absorption associated with those transitions. In the presence of an electromagnetic wave the electron and hole momenta become

$$\vec{p}_e + \frac{e}{c}\vec{A}(\vec{r}_e, t) , \tag{10}$$

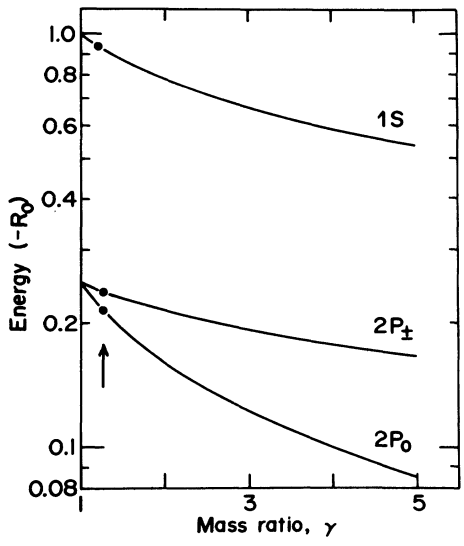

FIG. 1. Calculated $1S$, $2P_0$, and $2P_\pm$ energy levels as a function of the reduced-mass ratio, $\gamma = \mu_t/\mu_l$, of exciton in the high-stress limit. The vertical arrow indicates the value of γ for excitons in Ge. Notice, the hydrogen energy levels are given by $\gamma = 1$.

$$\vec{p}_h - \frac{e}{c}\vec{A}(\vec{r}_h, t) .$$

In the following, we will use the dipolar approximation and the Coulomb gauge. By using the above momenta the transformation (4) applied to the original Hamiltonian (1) give the same final H_{ex} in Eq. (6) except p_n is replaced by $p_n + (e/c)A_n$. After a few algebraic manipulations, the absorption coefficient α of electromagnetic radiation of the excitons is proportional to

$$\alpha \propto \nu_{if} |\sum_n \epsilon_n \langle i | x_n | f \rangle|^2 , \tag{11}$$

where ϵ is a unit polarization vector and ν_{if} is the transition frequency between the initial $|i\rangle$, and the final $|f\rangle$, state. Hence, for polarization, $\vec{E}$ parallel to the stress axis $\vec{E}||\vec{S}$, the only optical transition observed is from the $1S$ to $2P_0$ state. For polarization $\vec{E}$ perpendicular to the stress axis, $\vec{E}\perp\vec{S}$, the only optical transition observed is from the $1S$ to $2P_\pm$ states. The relative absorption of the $1S$-$2P_0$ transition to the $1S$-$2P_\pm$ transition is

$$\frac{\alpha_0}{\alpha_\pm} = \frac{\nu_0}{\nu_\pm}\left[\frac{\langle 1S | z | 2P_0 \rangle}{\langle 1S | x | 2P_\pm \rangle}\right]^2 . \tag{12}$$

An estimate of the matrix elements is obtained by using the variational wave functions. The relative absorption becomes

$$\frac{\alpha_0}{\alpha_\pm} \approx 1.4 . \tag{13}$$

The numerical value is expected to be accurate within a factor of 3—4 because of the variational method used. In Sec. IV, a comparison between the results developed here and the experiment will be given.

III. EXPERIMENTAL TECHNIQUES

Fourier-transform spectroscopy was used to study the absorption spectrum of excitons. A polarizing interferometer was used in conjunction with a doped germanium bolometer operating at 0.3 K to measure the absorption of excitons in the spectral region from 1 to 4 meV.

The sample was cut from a dislocation-free Ge crystal with a concentration of electrically active impurities $(N_A - N_D) \leq 2 \times 10^{11}$ cm^{-3}. The crystal was first oriented to within 0.5° by using the Laue method and cut along the [111], [11$\bar{2}$], and [1$\bar{1}$0] directions. The sample was mechanically polished and etched in CP4A solution (HNO_3, HF, CH_3COOH; 5:3:3) to reduce surface recombination. The crystal obtained was of dimensions 7.67 $\times 1.52 \times 2.17$ mm^3. The [11$\bar{2}$] face was wedged

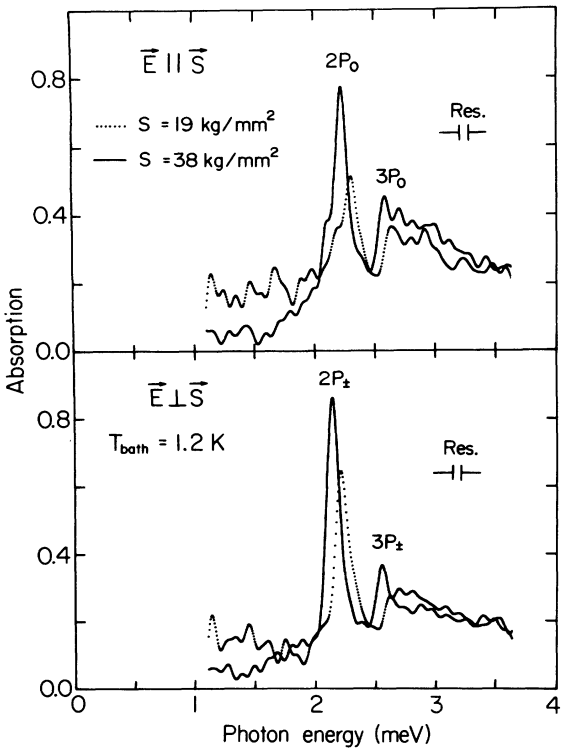

FIG. 2. Far-infrared absorption spectra of excitons in Ge as a function of uniaxial [111] stress. For each stress value a spectrum was taken with the FIR polarization parallel and perpendicular to the stress axis. The laser power was the same for all spectra. The labels in the spectra indicate the 1*S*-2*P* and 1*S*-3*P* transitions. Notice the shift in energy of the absorption lines as the stress increases. This shift is produced by a continuous decoupling of the valence bands.

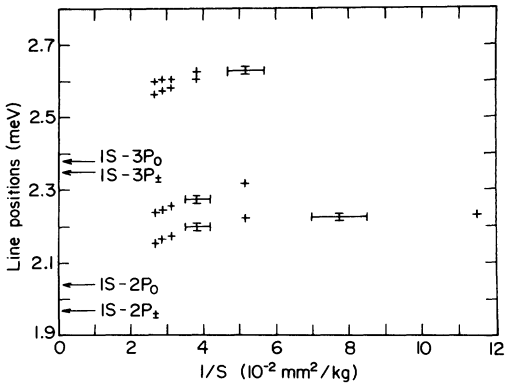

FIG. 3. Plot of the exciton line positions as a function of the reciprocal stress $1/S$. The horizontal arrows indicate the theoretical line positions at infinite stress. As the stress increases, the 1*S*-2*P* and 1*S*-3*P* transitions approach the theoretical line positions corresponding to the high-stress limit.

with an angle of 1.8° to remove any spurious reflections. The longest dimension was along the [111] direction. The [111] surfaces were not etched to avoid surface irregularities and, hence, stress inhomogeneities. The crystal was stressed between indium pads to produce good stress homogeneities and good thermal contacts.

The optical excitation was produced by a cw YAG:Nd (YAG denotes yttrium aluminum garnet) laser operating at a wavelength of 1.064 μm. The laser beam was focused to a 1-mm-diam beam size on the [11$\bar{2}$] surface and absorbed power by the sample was 8 mW. The stress apparatus is described elsewhere.[23] The stress could be varied from outside the cryostat. A capacitive stress sensor was used to calibrate the stress apparatus. Resulting stresses on the crystal range from 0 to 40 kg/mm^2. A rotatable polarizer consisting of a gold grid (1000 lines/in.) deposited on Mylar provides consecutively a polarization perpendicular $\vec{E}\perp\vec{S}$ and parallel $\vec{E}\|\vec{S}$ to the stress axis. The measured absorption is given by

$$\alpha d = \ln(I_0/I) ,$$

where I_0 (I) is the bolometer signal when the laser is off (on) and d is the thickness of the absorption region. All absorption spectra were taken with the sample immersed in liquid helium.

IV. EXPERIMENTAL RESULTS AND DISCUSSIONS

Measured absorption spectra of excitons are shown in Fig. 2. These spectra were taken at $T = 1.2$ K and for each stress value, a spectrum was taken with $\vec{E}\|\vec{S}$ and $\vec{E}\perp\vec{S}$. The laser power was the same for all spectra, hence the evolution in relative absorption can be observed. The upper part of Fig. 2 shows an absorption spectrum taken at $S = 19$ kg/mm^2 and $\vec{E}\|\vec{S}$. At this stress value the separation between the lower and upper conduction band is 19.6 meV. Hot excitons exist at lower stresses but at these high stresses intervalley scattering depopulates the upper states of Chou *et al.*[24] A strong line associated with the 1*S*-2P_0 transition at 2.32 meV is observed among several weak lines. Also observed in the spectrum is a shoulder located on the low-energy side of the 1*S*-2P_0 transition. The shoulder and the weak lines may be related to residual warping of the valence bands. The background observed at ~ 3 meV in the spectrum is caused by the absorption of electron-hole drop (EHD).[23] The same features are also observed in the spectrum with $\vec{E}\perp\vec{S}$. A strong-

absorption line observed at 2.22 meV is identified with the $1S$-$2P_{\pm}$ transition. As the stress increases from 9 to 38 kg/mm^2, the $1S$-$2P$ transitions shift toward lower energy due to the continuous decoupling of the valence bands. This decoupling is also reflected in the high-energy side of the $1S$-$2P$ transitions where the spectrum of the weak lines varies with stress. The absorption spectrum of excitons at stress $S \geq 19$ kg/mm^2 shows another transition located at ~ 2.6 meV which becomes sharper with stress. We interpret this absorption line as the $1S$-$3P$ transition. This transition also has a dependence on polarization. At $S = 38$ kg/mm^2, the ratio of absorptions in both polarizations of the $1S$-$2P$ transitions is 0.8 ± 0.1. The last ratio compares well with the theoretical estimate of $\alpha_0/\alpha_{\pm} \approx 1.4$.

In order to estimate the line positions at infinite stress, the $1S$-$2P$ and $1S$-$3P$ line positions as a function of reciprocal stress, $1/S$ are plotted in Fig. 3. Also shown are the theoretical line positions[25] for $1/S = 0$ mm^2/kg. The theoretical values are given in Table I. Notice the increase in curvature of the data points as $1/S$ goes to zero. The change of curvature suggests that the experimental line positions tend toward the theoretical ones as the stress increases. Furthermore, the observed splittings between the two sets of transitions $2P_0$-$2P_{\pm}$ and $3P_0$-$3P_{\pm}$ converge at high stress to the theoretical ones. An extrapolation of the data points to infinite stress was done. A comparison between the theoretical and extrapolated line positions is shown in Table I. Good agreement is obtained between theory and experiment. This agreement enables us to estimate the binding energy of excitons at infinite stress as 2.70 ± 0.08 meV. Thus, while there are problems in understanding the spectrum of free excitons at zero stress in the high-stress limit, the structure becomes nearly hydrogenlike and, hence, very simple to interpret.

TABLE I. Experimental and theoretical line positions of excitons in the high-stress limit.

Transition	Theory ν (meV)	Experimental[a] ν (meV)
$1S$-$2P_0$	2.04	2.09 ± 0.09
$1S$-$2P_{\pm}$	1.97	2.02 ± 0.08
$1S$-$3P_0$	2.38[b]	2.5 ± 0.2
$1S$-$3P_{\pm}$	2.35[b]	2.45 ± 0.2

[a]The line positions were obtained from an extrapolation of the data points to $1/S = 0$ mm^2/kg.
[b]See. Ref. 25.

ACKNOWLEDGMENTS

We would like to thank D. A. Goodings for several helpful discussions on the theoretical aspect of the problem. We would also like to thank E. E. Haller and W. L. Hansen for providing the Ge crystal and M. A. Paalanen for a fruitful discussion concerning the design of the stress sensor. This work was supported in part by the Natural Sciences and Engineering Research Council of Canada and by the Government of the Province of Ontario.

[1]E. M. Gershenzon, G. N. Gol'tsman, and N. G. Ptitsina, Zh. Eksp. Teor. Fiz. Pis'ma Red. 16, 228 (1972) [JETP Lett. 16, 161 (1972)].
[2]V. S. Vavilov, N. V. Guzeev, V. A. Zayats, V. L. Kononenko, T. S. Mandel'shtam, and V. N. Murzin, Zh. Eksp. Teor. Fiz. Pis'ma Red. 17, 480 (1973) [JETP Lett. 17, 345 (1973)].
[3]E. M. Gershenzon, G. N. Gol'tsman, and N. G. Ptitsina, Zh. Eksp. Teor. Fiz. Pis'ma Red. 18, 160 (1973) [JETP Lett. 18, 93 (1973)].
[4]N. V. Guzeev, V. A. Zayats, V. L. Kononenko, T. S. Mandel'shtam, and V. N. Murzin, Fiz. Tekh. Poluprovodn. 8, 1633 (1974) [Sov. Phys.—Semicond. 8, 1061 (1975)].
[5]E. M. Gershenzon, G. N. Gol'tsman, and N. G. Ptitsina, Zh. Eksp. Teor. Fiz. Pis'ma Red. 70, 224 (1976) [JETP Lett. 43, 116 (1976)].
[6]M. Buchanan and T. Timusk, *Proceedings of the Thirteenth International Conference of the Physics of Semiconductors, Rome, 1976,* edited by F. G. Fumi (Tipografia Marves, Rome, 1976), p. 821.
[7]H. Navarro, Ph.D. thesis, McMaster Unversity, 1979 (unpublished).
[8]V. I. Sidorov and Ya. E. Pokrovskii, Fiz. Tekh. Popuprovodn. 6, 2405 (1972) [Sov. Phys.—Semicond. 6, 2015 (1973)].
[9]A. Frova, G. A. Thomas, R. E. Miller, and E. O. Kane, Phys. Rev. Lett. 34, 1572 (1975).
[10]N. O. Lipari and M. Altarelli, Phys. Rev. B 15, 4883 (1977).
[11]M. Altarelli and N. O. Lipari, Phys. Rev. B 15, 4898 (1977).
[12]N. O. Lipari, M. Altarelli, and E. Tosatti, Solid State Commun. 21, 979 (1977).
[13]K. Muro and S. Narita, *Proceedings of the Thirteenth International Conference of the Physics of Semiconduct-*

ors, Rome, 1976, edited by F. G. Fumi (Tipografia Marves, Rome, 1976), p. 853.
[14]M. Yamanaka, K. Muro, and S. Narita, J. Phys. Soc. Jpn. 44, 1222 (1978).
[15]B. J. Feldman, H.-h. Chou, and G. K. Wong, Solid State Commun. 24, 521 (1977).
[16]B. J. Feldman, H.-h. Chou, and G. K. Wong, Solid State Commun. 26, 209 (1978).
[17]I. Balslev, Phys. Rev. 143, 636 (1966).
[18]J. C. Hensel and K. Suzuki, Phys. Rev. B 9, 4219 (1974).
[19]B. W. Levinger and D. R. Frankl, J. Phys. Chem. Solids 20, 281 (1961).
[20]R. A. Faulkner, Phys. Rev. 184, 713 (1969).
[21]W. Kohn and J. M. Luttinger, Phys. Rev. 98, 915 (1955).
[22]R. W. Keyes, IBM J. Res. Dev. 5, 65 (1961).
[23]H. G. Zarate and T. Timusk, Can. J. Phys. 60, 1008 (1982).
[24]H.-h. Chou, J. Bajaj, G. K. Wong, and B. J. Feldman, J. Lumin. 18/19, 573 (1979).
[25]The $3P_0$ and $3P_\pm$ energy levels were obtained by extrapolating Faulkner's calculation to a value of $\gamma^{1/3}=1.0843$. See Ref. 20.